Geophysical Research Letters

RESEARCH LETTER
10.1029/2021GL097070

How Does Land Cover and Its Heterogeneity Length Scales Affect the Formation of Summertime Shallow Cumulus Clouds in Observations From the US Southern Great Plains?

Jingjing Tian[1], Yunyan Zhang[1], Stephen A. Klein[1], Rusen Öktem[2,3], and Likun Wang[4]

[1]Lawrence Livermore National Laboratory, Livermore, CA, USA, [2]Department of Earth and Planetary Science, University of California, Berkeley, Berkeley, CA, USA, [3]Climate and Ecosystem Sciences Division, Lawrence Berkeley National Laboratory, Berkeley, CA, USA, [4]Cooperative Institute for Satellite Earth System Studies (CISESS), Earth System Science Interdisciplinary Center (ESSIC), University of Maryland, College Park, MD, USA

Abstract This study investigates the effects of heterogeneous land covers on shallow cumulus (ShCu) clouds at the US Southern Great Plains using high-resolution satellite and land cover data. During late summer, ShCu occurs over cities the most frequently and over open waters the least frequently, and more often over forest than over grassland. The preferential occurrence of ShCu over forest relative to grassland is consistent with surface measurements showing larger heat fluxes over forests. This preferential occurrence also varies with the length scales of land patches with the largest cloud occurrence difference shifting from smaller length scales (<9 km) during midday to larger scales (>9 km) in the early afternoon. Consistent with theory, these signals are more pronounced under low wind conditions. The preferential length scale shift with time suggests the existence of secondary circulations that strengthen and promote convergence over larger spatial scales as the differential land surface heating intensifies.

Plain Language Summary Continental shallow cumulus (ShCu) clouds are tightly coupled with the underlying heterogenous land cover. This study provides new evidence of the heterogenous land cover effect on ShCu formation using high resolution satellite cloud observations and land cover data at the US Southern Great Plains. During late summer, ShCu occurs over cities the most frequently and over open waters the least frequently, and more often over forest than over grassland. Observations further show that the cloud occurrence preference over forest relative to grassland varies with the length scales of land cover patches. More interestingly, the preferential length scale of cloud occurrence over forest shifts with time: the large cloud occurrence difference between forest and grassland is found at smaller spatial scales during midday, while at larger spatial scales in the early afternoon. These signals are more noticeable when winds calm down. The scale preferences of cloud occurrence difference between forest and grassland and their shift with time suggest that as the day progresses, the intensifying surface heating contrast between the adjacent forest and grassland patches may drive and strengthen secondary circulations, which promote convergence over larger and larger spatial scales and favor cloud formations over forest.

Key Points:

- Satellite observations indicate summertime shallow cumulus generally increase as one goes from lakes, to grassland, to forest and to cities
- Consistent with theory, the land cover effect on clouds varies with the length scales of patches and magnifies as wind speed decreases
- A cloud preference for forest rather than grassland shifts to larger scales as the day progresses, suggestive of secondary circulations

Supporting Information:

Supporting Information may be found in the online version of this article.

Correspondence to:

J. Tian,
tian5@llnl.gov

Citation:

Tian, J., Zhang, Y., Klein, S. A., Öktem, R., & Wang, L. (2022). How does land cover and its heterogeneity length scales affect the formation of summertime shallow cumulus clouds in observations from the US Southern Great Plains? *Geophysical Research Letters*, *49*, e2021GL097070. https://doi.org/10.1029/2021GL097070

Received 16 NOV 2021
Accepted 18 MAR 2022

Author Contributions:

Conceptualization: Jingjing Tian, Yunyan Zhang
Data curation: Jingjing Tian, Rusen Öktem, Likun Wang
Formal analysis: Jingjing Tian, Yunyan Zhang
Funding acquisition: Yunyan Zhang
Investigation: Jingjing Tian, Yunyan Zhang

1. Introduction

Continental shallow cumulus (ShCu) clouds are important for the surface energy balance and water budget because of their radiative and moistening effects and their seeding role to evolve into heavy-precipitating hot-tower clouds (Berg et al., 2011; Dong et al., 2005; Zhang & Klein, 2010, 2013). ShCu clouds are tightly coupled with the underlying land surface. The preference of cloud occurrence for different land cover types has been investigated in various ways, such as natural versus agricultural, forest versus deforested, and metropolitan versus rural (e.g., Carleton et al., 2001; Chagnon et al., 2004; Gambill & Mecikalski, 2011; Garcia-Carreras et al., 2017, 2010; Heiblum et al., 2014; Lyons et al., 1993; Nair et al., 2003; Rabin & Martin, 1996; Rabin et al., 1990; Ray et al., 2003; Theeuwes et al., 2019; J. Wang et al., 2009; Xu et al., 2022). For example, Gambill and Mecikalski (2011) found more ShCu clouds over forest than over its adjacent grassland at the southeastern United States, while in Europe Theeuwes et al. (2019) found less clouds over forest than over the nearby cities (e.g., Paris and London). Several mechanisms were proposed to explain the cloud occurrence preference over different land cover types:

Methodology: Jingjing Tian, Yunyan Zhang, Stephen A. Klein, Rusen Öktem, Likun Wang
Supervision: Yunyan Zhang
Visualization: Jingjing Tian
Writing – original draft: Jingjing Tian
Writing – review & editing: Jingjing Tian, Yunyan Zhang, Stephen A. Klein, Rusen Öktem, Likun Wang

1. Mean-State Difference: The difference in albedo, surface roughness, soil moisture content, and leaf area index among land covers (Bastable et al., 1993) leads to spatial variances in land surface energy budget and partitioning between the sensible and latent turbulent heating, thus impacts the evolution of atmospheric boundary layer and cloud formation (Betts, 2000).
2. Secondary Circulations: Differential heating of adjacent land cover patches can generate sea-breeze-like secondary circulations and induce mesoscale wind convergence, which affects the structure of planetary boundary layer (PBL) and promotes ShCu formation (Avissar & Liu, 1996; Avissar & Schmidt, 1998; Garcia-Carreras et al., 2010, 2011; Heinze et al., 2017; J. M. Lee et al., 2019; Pielke, 2001; Segal et al., 1988; Simon et al., 2021; Weaver & Avissar, 2001).

Many large-eddy simulation studies found that the secondary mesoscale circulations affecting convection and clouds can be induced when the land surface heterogeneities occur at a horizontal length scale, which is commonly suggested as 4–9 times of that of the PBL height (e.g., Avissar & Schmidt, 1998; Baidya Roy et al., 2003; Heinze et al., 2017; J. M. Lee et al., 2019; T. R. Lee et al., 2019; Patton et al., 2005; Van Heerwaarden & Teuling, 2014). However, there is limited observational evidence to confirm these modeling studies on the scale preference of the land cover effect on clouds (Garcia-Carreras et al., 2010; Taylor et al., 2007), because:

1. It is often not straightforward to define the surface heterogeneity length scale from observations (Baidya Roy et al., 2003; Garcia-Carreras et al., 2011; Taylor et al., 2007).
2. The secondary mesoscale circulations are difficult to observe directly (Asefi-Najafabady et al., 2012). The magnitude of secondary circulations and its impact on clouds may change diurnally as it is driven by the differential heating contrast in the diurnally varying land surface heat fluxes between adjacent patches with different heterogeneity length scales (Baidya Roy et al., 2003; Van Heerwaarden & Teuling, 2014). In the vicinity of the boundaries of heterogenous land covers, such phenomena are subtle and can be easily obscured by the effects of topography or strong winds (Doran et al., 1995; Garcia-Carreras et al., 2010; Kang et al., 2007; J. M. Lee et al., 2019; T. R. Lee et al., 2019; Lothon et al., 2011; Mahrt et al., 1994; Taylor et al., 2007; Weaver & Avissar, 2001; Zhong & Doran, 1997).
3. It is challenging to observe the diurnal cycles of small (sub-kilometer or kilometer scale) and short-lived (15 min of a life cycle) ShCu (Romps et al., 2021) due to instruments' coarse resolution or limited temporal/spatial coverage (e.g., polar-orbiting satellite or ground-based radar/lidar).

Thus, observational investigations on the impact of heterogenous land covers on ShCu clouds demand a clear definition of land heterogeneity length scale, as well as continuous cloud data of high temporal and spatial resolutions over vast areas of mixed land cover types, to characterize the response of clouds to the diurnally varying differential heating and secondary circulations.

The US Southern Great Plains (SGP) region is a favorable spot to study continental ShCu owing to the long-term co-located observations of land surface, atmospheric boundary layer and clouds by the Department Of Energy (DOE) Atmospheric Radiation Measurement (ARM) program (Berg & Kassianov, 2008; Kassianov et al., 2019; Lamer & Kollias, 2015; Lareau et al., 2018; Qiu & Williams, 2020; Romps & Öktem, 2018; Q. Tang et al., 2018; S. Tang et al., 2019; Xiao et al., 2018; Zhang & Klein, 2010, 2013; Zhang et al., 2017). Tao et al. (2019, 2021) showed that the observed low-level clouds at SGP strongly couple with the land surface properties and the late summer Cloud Fraction (CF) is larger in a region dominated by forest coverage than that dominated by grassland. Using Geostationary Operational Environmental Satellite (GOES-16) reflectance data, Tian et al. (2021) developed a method to detect ShCu around the SGP region (at a resolution of 650-m every 5 min), which may help shed light on the heterogeneity effect on clouds when paired with high resolution land cover data (Boryan et al., 2011). In this study, we take advantage of the newly developed GOES-16 ShCu data in Tian et al. (2021) and zoom into a region in the vicinity of SGP with mixed land cover types (mainly forests and grasslands) to answer two questions: (a) Does the ShCu occurrence differentiate among land cover types at the SGP? (b) Does ShCu occurrence depend on the heterogeneity length scale of land cover?

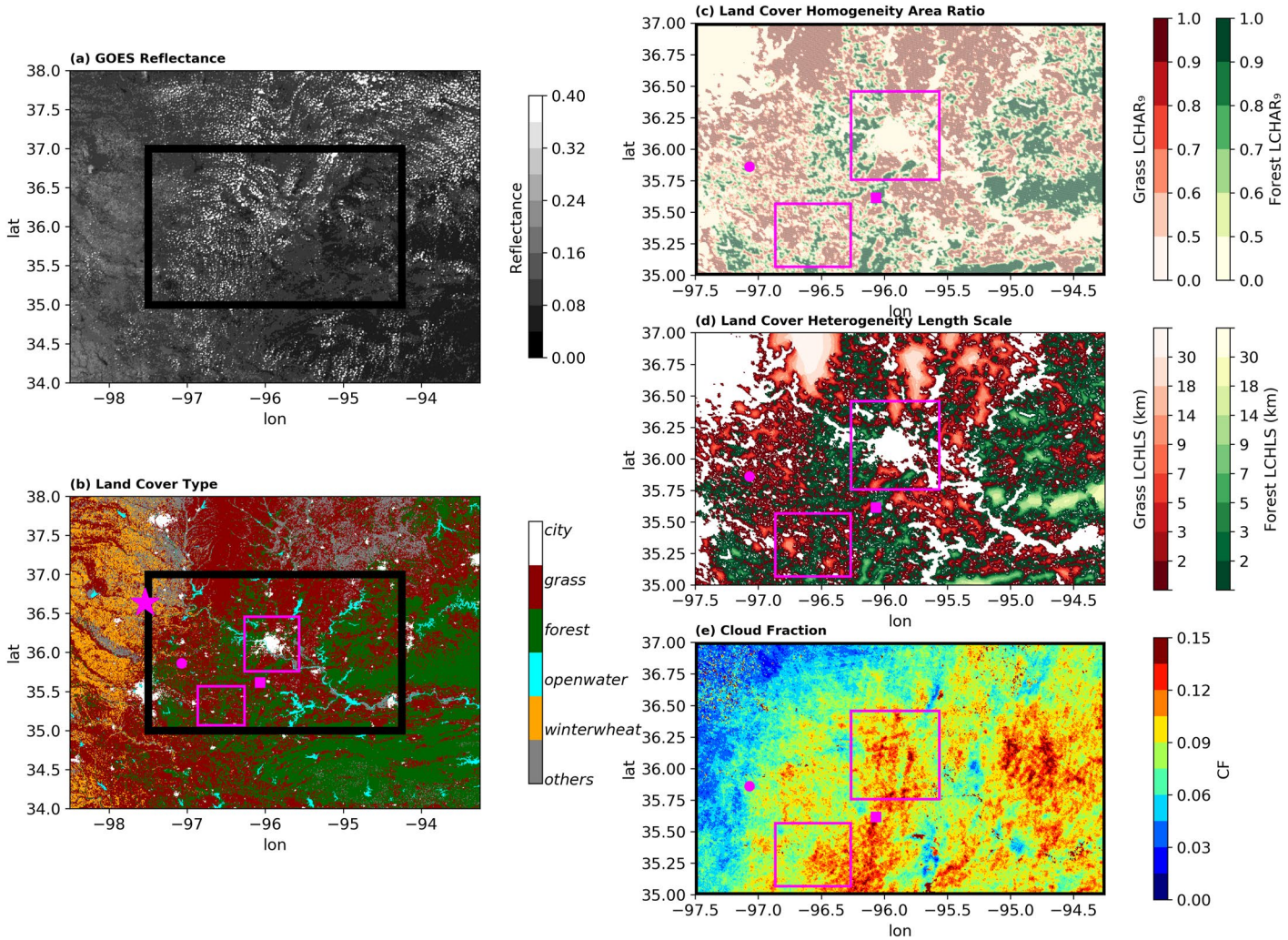

Figure 1. (a) An example image of Geostationary Operational Environmental Satellite reflectance data of shallow cumulus; (b) Land cover types (city/human development area; grassland/pasture; forest; open water; winter wheat; others) denoted by different colors; (c) The calculated land cover homogeneity area ratio within each land pixel's surrounding area of 9^2-km^2; (d) The calculated Land Cover Heterogeneity Length Scale and (e) Average cloud fraction at each land surface pixel (650-m resolution) calculated from 5-min reflectance data on the 17 fair-weather ShCu days. Black rectangle boxes in (a and b) represent the analysis domain in this study. Magenta stars in (b) show the location of Department of Energy Atmospheric Radiation Measurement Southern Great Plains central facility. Magenta circles (square) in (b–e) denote the extended facility E35 (E21) over grassland (forest). Small magenta boxes in (b–e) represent the two small-area transition zones: urban-to-rural (upper) and forest-to-grassland (lower).

2. Data and Methods

2.1. Detection of Shallow Cumulus

In this study, the analysis domain (Figure 1) is chosen according to Tao et al. (2019), which is about 220 km (north to south) by 300 km (west to east) with (a) mixed-types (mainly forests and grasslands/pastures with cities and lakes, negligible winter wheats nor other crops) and mixed-sizes of land cover patches and (b) small variations of surface elevation (Figure S1 in Supporting Information S1). During May to June, the large-scale atmospheric control provides spatially varying conditions across the SGP on days of shallow cumulus (Tao et al., 2019). Therefore, in this study we choose to focus on ShCu in later summer (July and August), during which the influence of the large-scale is more homogeneous across the analysis domain. Using animations of satellite images (https://satcorps.larc.nasa.gov/), we select 17 fair-weather ShCu days during July–August in 2018 and 2019 (Tao et al., 2019; Zhang & Klein, 2013). On these days, ShCu usually forms in the analysis domain rather widespread with the daytime cumulative domain mean precipitation less than 1 mm, based upon 4-km resolution surface precipitation data from Arkansas-Red Basin River Forecast Center (Fulton et al., 1998). Case selection also excludes large-scale weather systems, thus ShCu developments are strongly tied to land surface forcing and boundary layer processes.

To detect ShCu, we follow Tian et al. (2021) and use the 5-min reflectance data in the "red" visible channel from the GOES-16 cloud and moisture imagery data product (Schmit et al., 2010; Wu & Schmit, 2019). In the SGP region, the spatial resolution of the data is about 650 m (Figure 1a). A ShCu cloudy pixel is identified when the GOES reflectance exceeds the clear-sky surface reflectance by a ShCu reflectance detection threshold ($\Delta R = 0.045$), which was cross-validated with the observations of ShCu 3D morphology by the ground-based stereo cameras (Romps & Öktem, 2018) at the ARM SGP site (see Tian et al., 2021 for details). The sensitivity of ShCu detection to the values of ΔR is discussed in supplemental materials (Figure S2 in Supporting Information S1). Figure 1e displays the spatial distribution of CF, which is defined at each land surface pixel (e.g., 650-m resolution) as the probability of being identified as "cloudy" from all the available 5-min reflectance data for that pixel on the fair-weather ShCu days. Smaller CFs are seen over regions in the vicinity of open waters.

2.2. Land Cover Heterogeneity Length Scale

The land cover map with a 30-m spatial resolution in year 2018 (Figure 1b) is taken from the Cropland Data Layer data set by CropScape. This map is generated mainly based on 30-m Landsat observations (Boryan et al., 2011). Using this map, we define a variable called the land cover homogeneity area ratio ($LCHAR_x$) (Figure 1c) as the area ratio of a certain land cover type in this pixel's surrounding area of x^2-km^2 (or πR^2-km^2, where R is the radius) (Figure S3 and Text S1 in Supporting Information S1). $LCHAR_x$ characterizes the extent of land cover homogeneity (or heterogeneity) and helps us further define the local heterogeneity length scale. At each GOES pixel, we calculate its $LCHAR_x$ values with x(i) equal to 2, 3, 5, 7, 9, 14, 18, 30 km. These scales are selected following the heterogeneity length scales often used in the large eddy simulation studies (J. M. Lee et al., 2019). Among these scales, we find the largest x(i) for which the regional LCHAR > 0.95, and the land pixel is considered as belonging to a zone with Land Cover Heterogeneity Length Scale (LCHLS) between this largest scale x(i) and the next scale x(i+1) (Text S1 in Supporting Information S1). Figure 1d shows the map of LCHLS calculated for forest and grassland types. A larger LCHLS represents a land pixel close to the center of a large-size land cover patch, while a smaller LCHLS indicates a land pixel close to the land cover type boundaries. Sensitivity study shows that the following results are robust with different LCHAR thresholds used (0.98, 0.95 or 0.9) to define LCHLS.

2.3. Winds

It is necessary to consider the impact of winds in this analysis because strong winds: (a) may displace the cloud fields from its originating surface location, for example, downwind effect; (b) could give rise to more shear generated turbulence so that cloud occurrence may become less dependent on land cover; (c) may counteract with the induced secondary mesoscale circulations due to differential heating and alleviate the effect of land surface heterogeneities (J. M. Lee et al., 2019; Walker et al., 2009). In the following analysis, among the total 17 fair-weather ShCu days, 8 low-wind days are distinguished with the daytime domain average wind speed less than 3 m s^{-1}. Wind data are taken from the hourly 3-km resolution High Resolution Rapid Refresh analysis (Benjamin et al., 2016; Smith et al., 2008) and their uncertainty is less than 0.3 m s^{-1} (T. R. Lee et al., 2019).

2.4. Surface Measurements

Surface observations are from two extended facilities at the DOE ARM SGP site: E21 over forest and E35 over grassland. Best-estimate sensible and latent heat fluxes are from energy balance Bowen ratio (EBBR) at E35 (http://www.arm.gov/data/vaps/baebbr) and quality-controlled eddy correlation flux (ECOR) measurements at E21 (http://www.arm.gov/data/vaps/qcecor). The EBBR and ECOR systems also provide friction velocity, surface air pressure, temperature and relative humidity (RH), based on which Lifting Condensation Level (LCL) is estimated (Romps, 2017). Surface albedo is calculated using Quality Assessment for ARM Radiation Data (https://www.arm.gov/capabilities/vaps/qcrad). At E21, ECOR and radiation instruments are installed on a tower (15 m above ground and 3 m above the canopy) deployed in a deciduous oak forest. Although E21 and E35 are not located in the middle of the largest patches of forest and grassland in the analysis domain, the heat flux measurements from both EBBR and ECOR are representative of the surrounding land cover characteristics because of the sufficient fetch lengths, for example, homogenous forest and grassland within 1 km over 360° directions (Cook, 2018a; Cook, 2018b; S. Tang et al., 2019).

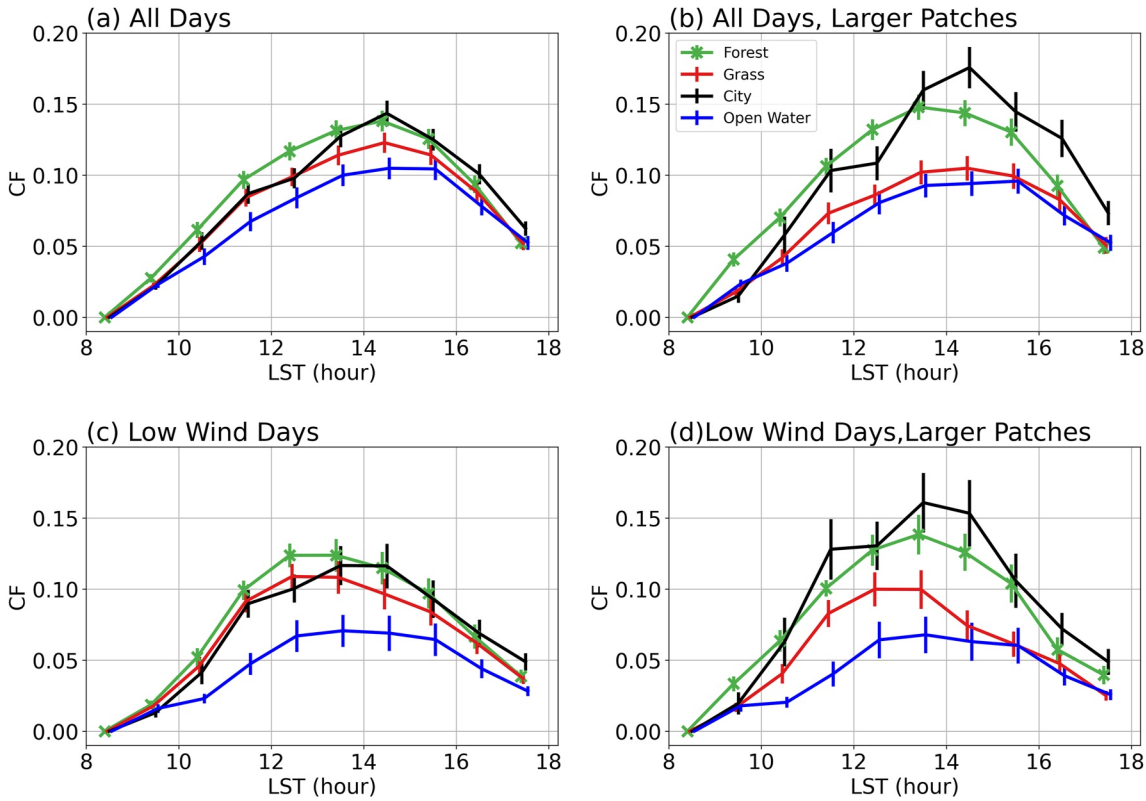

Figure 2. Diurnal evolutions of (a) cloud fraction over forest (green with cross), grassland (dark red), city (black) and open water (dark blue) in the analysis domain. The length of the vertical bars donates two standard errors of samples. (b) same as in (a) expect for larger patches (>5 km). (c and d) are the same as (a and b) but for low wind days.

3. Diurnal Variations of Clouds Over Different Land Cover Types

From the spatial plot (Figure 1e), it is easily to tell that CFs are small over open waters, however it is hard to directly recognize which land cover type favors larger CFs, among forest, grassland (pasture), and city (human development area). Figure 2 compares the diurnal cycles of CF over different land covers. CF as a function of time and land cover is calculated for each land cover type using 5-min satellite images. The length of the vertical bars in Figure 2 denotes two standard errors (~68% confidence interval) of 15-min average CF samples, which are considered independent according to the observed life cycle of ShCu (10–15 min) from ground-based stereo cameras at the SGP (Romps et al., 2021).

Figure 2a shows the comparison using all the ShCu cases and all the land pixels regardless of their LCHLS values. The CF shows a diurnal peak around 1430 Local Standard Time (LST) over all the land cover types. Consistent with Figure 1e, the smallest CFs are found over open waters during all the daytime hours. The CF over forest is larger than that over grassland in general, however the differences are statistically significant marginally. In the following we are going to examine the impact of LCHLS and wind speed on this comparison.

Figure 2b displays the CF comparisons over larger patches greater than 5 km. The city patch is over Tulsa, OK (a small urban area about 20 by 20 km mainly surrounded by forests and grasslands) in the analysis domain. Compared to Figure 2a, the city effect is the most pronounced with the largest CF especially in the afternoon. The differences in CF over larger patches between forest and grassland may increase to as large as 6 times the standard error and are much larger than those in the case of all land pixels (Figure 2a).

Figure 2c illustrates the wind speed effect in which CFs are from low wind cases. It is clearly noticed that the CFs over open waters decrease the most (also see Figure S3 in Supporting Information S1). The timing of CFs reaching 0.05 over open waters lags those of other land covers by about 1.5 hr, suggesting the slowest cloud development over open waters under low wind conditions. The CFs from low-wind cases are generally smaller than those

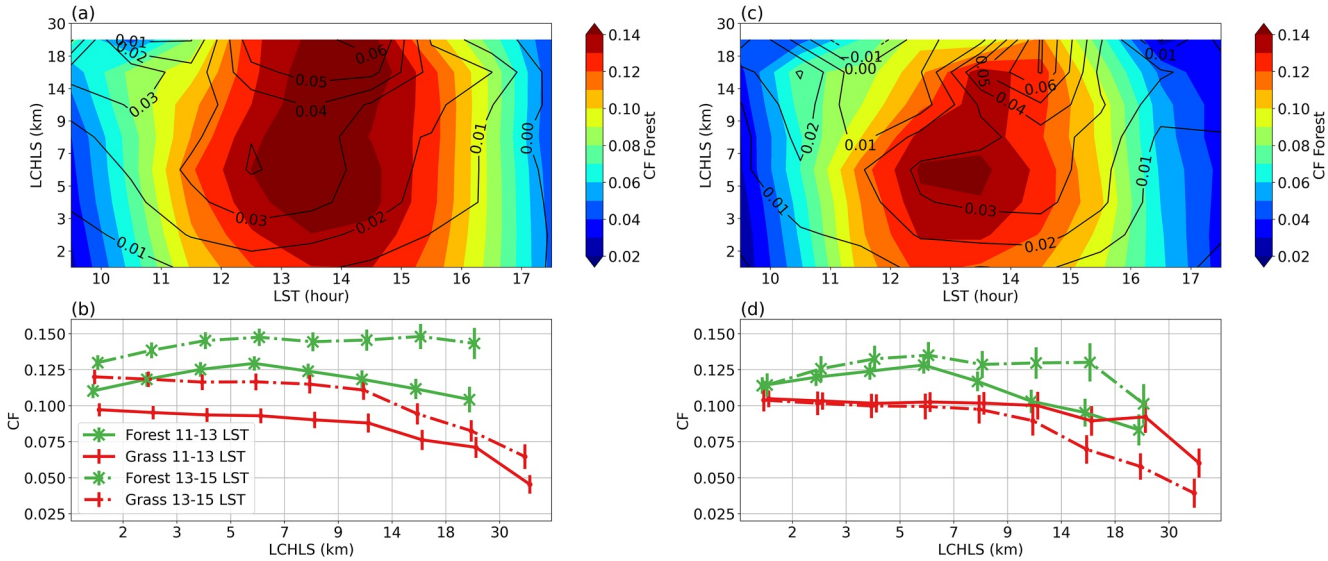

Figure 3. (a) Cloud fraction (CF) over forest as a function of local time and land cover heterogeneity length scale (LCHLS). Solid black contour lines represent the CF difference between forest and grassland. (b) Mean CFs over forest (green with cross) and grassland (red) during 11–13 local solar time (LST) (solid line) and 13–15 LST (dashed dot line). The length of the vertical bars donates two standard errors of 15-min mean CFs in each LCHSL bin. (c and d) are the same as (a and b) expect for low wind cases.

based on all the cases (Figure 2a), possibly because stronger winds, usually Southerlies (Song et al., 2019), bring a larger moisture transport from Gulf of Mexico and also enhance greater surface heat fluxes (Liu et al., 2013) to favor cloud formation. It is also noticed that CFs of low winds over forest and grassland tend to peak much earlier, for example, at 1230 LST compared to 1430 LST of all the cases (Figure 2a).

Figure 2d shows the joint effect of larger land cover patches and low wind speeds. The effects of city and open water are the most distinguishable (Figure S4 in Supporting Information S1). Reasons for this preference are discussed in Text S2 in Supporting Information S1. Over forest and grassland, their CF difference increases from morning to afternoon and becomes much more significant after 1300 LST.

In addition to Figure 2, CF changes across land cover boundaries. We carefully zoom into two small areas with land cover transitions (Figure 1, magenta boxes) and find that: (a) the largest CF occurs over the city center of Tulsa, OK while decreasing when moving away from the city center toward the adjacent rural areas (Figure S5 in Supporting Information S1 and Movie S1); (b) the largest CF occurs over the center of a forest belt while decreasing toward the adjacent grasslands (Figure S6 in Supporting Information S1 and Movie S2).

4. Preference of ShCu Occurrence on Land Cover Heterogeneity Length Scale

In this section, we focus on the impact of the heterogeneity length scales of forest and grassland, the two dominate land covers often mixed with each other in the analysis domain (Figures 1b–1d). CF is calculated as a function of time and LCHLS for forest and grassland. For each 5-min satellite image, we calculate mean CFs at every LCHLS using number of cloudy pixels dividing the total land pixel number at given LCHLS, and then based on the time-series of CFs, we calculate the hourly means.

Figure 3a shows the diurnal variations of ShCu CFs over forest at different length scales for all cases (see Figure S7 in Supporting Information S1 for CFs over grassland). During midday (1100–1300 LST), the CF over forest peaks at 5–7 km (noticed from the vertical slant of the boundaries between different colors). Such signal is more clearly observed from the low wind case composite (Figure 3c). While after 1330 LST, the boundaries between different colors of CF become more straight vertically, and CFs are almost the same at different scales.

Figure 3d further extracts the mean CFs over forest and grassland during two periods: midday (1100–1300 LST) and early afternoon (1300–1500 LST) for low wind cases. In Figure 3d, during midday, the CF difference between forest and grassland stands out at smaller length scales (<9 km) with the largest contrast around 5–7 km,

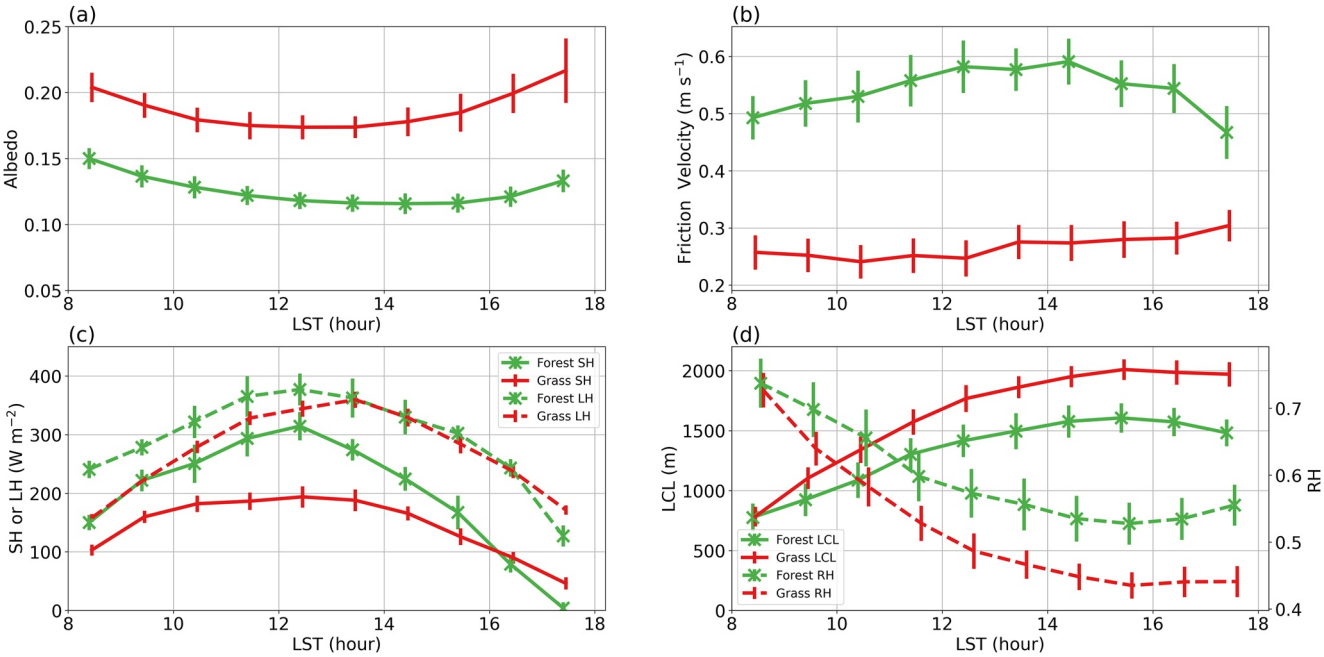

Figure 4. Diurnal evolutions of (a) surface albedo, (b) friction velocity, (c) sensible heat flux (solid) and latent heat flux (dashed); and (d) lifted condensation level (solid) and relative humidity (dashed) at E21 (forest, green with cross) and E35 (grassland, red), the extended facilities of the Department of Energy Atmospheric Radiation Measurement Southern Great Plains site. The length of the vertical bars denotes two standard errors across all the samples.

however at the larger heterogeneity length scales (>9 km), CFs are almost equal over forest and grassland. The CF difference between forest and grassland peaks at 5–7 km during midday, suggesting that the strongest impact of secondary mesoscale circulations on cloud occurs when the ratio of heterogeneity length scale relative to PBL height is between 4 and 9. This in general agrees with Patton et al. (2005), in which strongest patch-induced circulations correspond to heterogeneity length scales between 4 and 9 km if the PBL depth is about 1 km.

From midday to early afternoon, the CF increases over forest but decreases over grassland, especially in the areas with larger heterogeneity length scales (>9 km). Such shifts result in the CF difference between forest and grassland increasing with the heterogeneity length scale in the early afternoon, opposite to that during midday. For example, the CF difference is 0.03 (0.13 vs. 0.10) around 5–7 km during midday but increases to 0.06 (0.13 vs. 0.07) around 14–18 km in early afternoon. These differences are compelling, which are much larger than those differences without length scale separations (Figures 2a and 2c).

For the composite of all the cases without wind speed filtering (Figure 3b), at midday the CF differences between forest and grassland are almost constant when LCHLS > 5 km. From midday to early afternoon, the CF increases over both forest and grassland, and the scale preference shift is weaker in the composite using all the cases (Figure 3b) as compared with the one based on low wind cases (Figure 3d).

5. Discussion on the Relative Preference of Clouds Over Forest Versus Grassland

In this section, we will explore if in situ surface station observations support the findings in Sections 3 and 4: (a) a more frequent ShCu occurrence over forest than over grassland; (b) a shift of the length scale preference of cloud occurrence difference from midday to early afternoon.

5.1. Surface Turbulent Fluxes Impact PBL and LCL

Figure 4 show the composite diurnal evolution of surface albedo, friction velocity, sensible and latent heat fluxes, LCL and RH from surface observations at the forest (E21) and grassland (E35) DOE ARM sites. The forest site has a lower albedo and absorbs more solar energy than the grassland site (Figure 4a) (Berg et al., 2020). The forest site also has a rougher canopy (Mahrt & Ek, 1993) and larger friction velocity (Figure 4b), promoting an

efficient exchange of heat, moisture and momentum, and tempering the surface temperature, thereby reducing outgoing longwave radiation (Teuling et al., 2017). Lower albedo and larger roughness can result in larger net radiation over forest, which can be used for evapotranspiration and for warming the atmosphere. Figure 4c shows larger sensible as well as latent heat fluxes over forest (S. Tang et al., 2019; Tao et al., 2019; Teuling et al., 2010).

Before 1600 LST, sensible heating is 30%–50% larger over forest than over grassland. This results in a more rapid development of PBL over forest and at the meantime brings more dry air into the PBL. Such development couples with turbulence driven by land surface sensible heat fluxes and usually maintains until late afternoon (1600 LST).

Early morning (0830 LST) RH near surface is found very similar over forest and grassland, thus similar initial LCL heights calculated based on RH (Figure 4d). At the same time, the early morning latent heat flux over forest is about 60% larger than over grassland, although the difference becomes smaller through early afternoon (1330 LST). This supplies stronger moistening of boundary layer over forest. Such moistening is reflected in the behavior of LCL. The derived LCL over forest is always lower by several hundred meters than that over grassland and such difference also increases with time. Before 1300 LST, LCL increases rapidly due to the strong PBL top entrainment drying, while after 1300 LST, the PBL humidity tends to remain a balance thus LCL levels out in the afternoon.

The onset of shallow cumulus is triggered by vigorous PBL development reaching LCL (Gentine et al., 2013; Y. Wang et al., 2020; Wilde et al., 1985). In this study, larger net radiation and roughness over forest leads to stronger sensible and latent heat fluxes, which result in faster PBL development and lower LCL, thus a larger CF than over grassland. While this mechanism may support the CF difference between forest and grassland, it alone cannot explain the length scale preference of clouds and the shift from midday to early afternoon in the scale preference of the cloud occurrence difference.

5.2. Differential Surface Heating Induces Secondary Circulations

What if the large difference in surface heating ($\sim$100 Wm^{-2} of sensible heat flux difference at local noon between forest and grassland) is found between adjacent patches of different length scales? Differential heating between adjacent patches may induce secondary mesoscale circulations, which further promote convergence and reinforce the cloud formation (Garcia-Carreras et al., 2010, 2011; J. M. Lee et al., 2019; Rieck et al., 2014). If there are no secondary circulations, we would expect similar CF difference between forest and grassland at different heterogeneity length scales. However, Figure 3d clearly shows that the CF difference between forest and grassland changes with heterogeneity length scale, which suggests the existence of secondary circulations.

In addition, there is a shift of the largest CF difference between forest and grassland from smaller scales (<9 km) during 1100–1300 LST to larger length scales (>9 km) during 1300–1500 LST. Such shift happens around the diurnal peak time (1230 LST) of sensible heat fluxes and their differences between forest and grassland (Figure 4c). This suggests not only an intensification of secondary circulations from midday to early afternoon but also a slight time lag between the peak differential heating and the effect of secondary circulations on cloud occurrence. This is because the maximum surface air temperature usually lags the diurnal peak surface sensible heat flux, and it also takes time for secondary circulations to develop and travel across patch boundaries and form convergence zones. For example, large-eddy simulations suggest with no background winds, it takes about 1.5 hr to travel 8 km (half size of a patch of 16 km wide) to create a convergence zone (at the center of the patch) with a horizonal speed of secondary circulations at 1.5 m/s (J. M. Lee et al., 2019). This may help explain the early-afternoon shift of the largest CF difference between forest and grassland to a larger heterogeneity scale, for example, 14–18 km. Also, the horizonal speed of secondary circulations is usually associated with the magnitude of heat fluxes and the heating contrast between adjacent heterogeneous areas (Baidya Roy et al., 2003). Thus, as differential heating intensifies from morning to noon (Figure 4c), the induced secondary circulations become stronger to promote convergence at larger patches.

6. Conclusions

This study provides new observational evidence to support the land cover effect on shallow cumulus cloud formation, using high-resolution geostationary satellite observations, land cover data and the DOE ARM SGP surface measurements. During late summer (July and August), ShCu prefers to occur least over open waters and most

over city especially in the late afternoon. ShCu is more likely to occur over forest than over grassland: during midday, the largest CF difference occurs at smaller heterogeneity length scales (<9 km), while in the early afternoon, the largest difference shifts toward larger heterogeneity length scales (>9 km).

Our findings on the preference of cloud occurrence over forest than over grassland are supported by surface measurements, which show both larger sensible and latent heat fluxes over forest, indicating a more rapid development of PBL and a much lower LCL. We further speculate that the shift of the scale preference of cloud occurrence difference over forest before and after the diurnal peak timing of surface heat fluxes is associated with the development of secondary circulations, in which as differential heating intensifies, the secondary circulations become stronger to converge over larger spatial scales. Such shift of scale preference is more pronounced under low wind conditions when background winds is not strong enough to suppress secondary circulations.

The land cover effect on ShCu is a complex interplay. Results of this study should be used with caution when extrapolated to other forest areas with different surface characteristics, for example, a smaller sensible heat flux than their surroundings (Fisch et al., 2004). The effect on cloud formation may also distinguish among forest types (Duveiller et al., 2021), for example, the access to deep soil water (Ek & Holtslag, 2004) or the emissions of biogenic volatile organic compounds (Kulmala et al., 2004; Peñuelas & Staudt, 2010) may also play a role. Soil moisture can also affect the turbulent heating over forest and grassland. Even though no large soil moisture difference are observed from site observations in the analysis domain, the soil moisture effect on cloud formation cannot be excluded (Chen et al., 2020; Findell & Eltahir, 2003; Pielke, 2001; Sakaguchi et al., 2022; Taylor et al., 2011, 2012). More advanced observations (e.g., soil moisture network, collocated boundary layer and cloud profiling) and high-resolution numerical simulations with improved representations of clouds, atmospheric boundary layer, and land properties are needed to attribute the relative contributions of these intertwining processes (Beamesderfer et al., 2022).

Clouds and convection are usually coupled with land surfaces through grid-mean surface fluxes in climate models (10–100 km resolution). The land cover scale preference of ShCu occurrence over forest relative to grassland suggests that the sub-grid scale interactions between land surface, atmospheric boundary layer and clouds need to be considered to improve the model representations of convection and precipitation processes over land at diurnal scales. The framework and data developed in this study can be further applied to investigate shallow to deep convective cloud transition processes and their interactions with land covers.

Data Availability Statement

Data used in this study are from the U.S. Department Of Energy as part of the Atmospheric Radiation Measurement (ARM) Climate Research Facility Southern Great Plains site: EBBR and quality-controlled eddy correlation flux data are downloaded at http://www.arm.gov/data/vaps/baebbr and http://www.arm.gov/data/vaps/qcecor. ARM radiation data are downloaded at https://www.arm.gov/capabilities/vaps/qcrad. NOAA satellite GOES-R Series ABI Product is from NOAA CLAss at https://www.avl.class.noaa.gov/saa/products/search?sub_id=0&datatype_family=GRABIPRD&submit.x=30&submit.y=13. The High Resolution Rapid Refresh (HRRR) analysis and forecast data products were obtained from the HRRR archive at University of Utah (http://hrrr.chpc.utah.edu/; https://doi.org/10.7278/S5JQ0Z5B).

Acknowledgments
The authors sincerely thank David Romps for discussions on the shallow cumulus cloud detection. J. Tian was supported by the Department Of Energy (DOE) Office of Science Early Career Research Program awarded to Y. Zhang. Y. Zhang, S. A. Klein and R. Oktem acknowledge support by the DOE Atmospheric System Research program. L. Wang acknowledges support from NOAA grant NA19NES4320002 (Cooperative Institute for Satellite Earth System Studies) at the University of Maryland/Earth System Science Interdisciplinary Center. Lawrence Livermore National Laboratory is operated by Lawrence Livermore National Security, LLC, for the U.S. DOE under contract DE-AC52-07NA27344.

References

Asefi-Najafabady, S., Knupp, K., Mecikalski, J. R., & Welch, R. M. (2012). Radar observations of mesoscale circulations induced by a small lake under varying synoptic-scale flows. *Journal of Geophysical Research*, *117*(1), D01106. https://doi.org/10.1029/2011JD016194

Avissar, R., & Liu, Y. (1996). Three-dimensional numerical study of shallow convective clouds and precipitation induced by land surface forcing. *Journal of Geophysical Research*, *101*(D3), 7499–7518. https://doi.org/10.1029/95JD03031

Avissar, R., & Schmidt, T. (1998). An evaluation of the scale at which ground-surface heat flux patchiness affects the convective boundary layer using large-eddy simulations. *Journal of the Atmospheric Sciences*, *55*(16), 2666–2689. https://doi.org/10.1175/1520-0469(1998)055<2666:AEOTSA>2.0.CO;2

Baidya Roy, S., Weaver, C. P., Nolan, D. S., & Avissar, R. (2003). A preferred scale for landscape forced mesoscale circulations? *Journal of Geophysical Research*, *108*(22), 1–11. https://doi.org/10.1029/2002jd003097

Bastable, H. G., Shuttleworth, W. J., Dallarosa, R. L. G., Fisch, G., & Nobre, C. A. (1993). Observations of climate, albedo, and surface radiation over cleared and undisturbed Amazonian forest. *International Journal of Climatology*, *13*(7), 783–796. https://doi.org/10.1002/joc.3370130706

Beamesderfer, E. R., Buechner, C., Faiola, C., Helbig, M., Mayari Sanchez-Mejia, Z., María Yáñez-Serrano, A., et al. (2022). Advancing cross-disciplinary understanding of land-atmosphere interactions. *Journal of Geophysical Research: Biogeosciences*, *127*, e2021JG006707. https://doi.org/10.1029/2021JG006707

Benjamin, S. G., Weygandt, S. S., Brown, J. M., Hu, M., Alexander, C. R., Smirnova, T. G., et al. (2016). A North American hourly assimilation and model forecast cycle: The rapid refresh. *Monthly Weather Review*, *144*(4), 1669–1694. https://doi.org/10.1175/MWR-D-15-0242.1

Berg, L. K., Berkowitz, C. M., Barnard, J. C., Senum, G., & Springston, S. R. (2011). Observations of the first aerosol indirect effect in shallow cumuli. *Geophysical Research Letters*, *38*(3), 1–5. https://doi.org/10.1029/2010GL046047

Berg, L. K., & Kassianov, E. I. (2008). Temporal variability of fair-weather cumulus statistics at the ACRF SGP site. *Journal of Climate*, *21*(13), 3344–3358. https://doi.org/10.1175/2007JCLI2266.1

Berg, L. K., Long, C. N., Kassianov, E. I., Chand, D., Tai, S. L., Yang, Z., et al. (2020). Fine-scale variability of observed and simulated surface albedo over the Southern Great Plains. *Journal of Geophysical Research: Atmospheres*, *125*(7), 1–14. https://doi.org/10.1029/2019JD030559

Betts, A. K. (2000). Idealized model for equilibrium boundary layer over land. *Journal of Hydrometeorology*, *1*(6), 507–523. https://doi.org/10.1175/1525-7541(2000)001<0507:imfebl>2.0.co;2

Boryan, C., Yang, Z., Mueller, R., & Craig, M. (2011). Monitoring US agriculture: The US department of agriculture, national agricultural statistics service, cropland data layer program. *Geocarto International*, *26*(5), 341–358. https://doi.org/10.1080/10106049.2011.562309

Carleton, A. M., Adegoke, J., Allard, J., Arnold, D. L., & Travis, D. J. (2001). Summer season land cover-Convective cloud associations for the midwest U.S "Corn Belt." *Geophysical Research Letters*, *28*(9), 1679–1682. https://doi.org/10.1029/2000GL012635

Chagnon, F. J. F., Bras, R. L., & Wang, J. (2004). Climatic shift in patterns of shallow clouds over the Amazon. *Geophysical Research Letters*, *31*(24), 1–4. https://doi.org/10.1029/2004GL021188

Chen, J., Hagos, S., Xiao, H., Fast, J. D., & Feng, Z. (2020). Characterization of surface heterogeneity-induced convection using cluster analysis. *Journal of Geophysical Research: Atmospheres*, *125*(20), 1–16. https://doi.org/10.1029/2020JD032550

Cook, D. R. (2018a). *Energy balance bowen ratio station (EBBR) instrument handbook*. https://doi.org/10.2172/1020562

Cook, D. R. (2018b). *Eddy correlation flux measurement system (ECOR) instrument handbook*. https://doi.org/10.2172/1467448

Dong, X., Minnis, P., & Xi, B. (2005). A climatology of midlatitude continental clouds from the ARM SGP central facility: Part I: Low-level cloud macrophysical, microphysical, and radiative properties. *Journal of Climate*, *18*(9), 1391–1410. https://doi.org/10.1175/JCLI3342.1

Doran, J. C., Shaw, W. J., & Hubbe, J. M. (1995). Boundary layer characteristics over areas of inhomogeneous surface fluxes. *Journal of Applied Meteorology*, *34*(2), 559–571. https://doi.org/10.1175/1520-0450-34.2.559

Duveiller, G., Filipponi, F., Ceglar, A., Bojanowski, J., Alkama, R., & Cescatti, A. (2021). Revealing the widespread potential of forests to increase low level cloud cover. *Nature Communications*, *12*(1), 4337. https://doi.org/10.1038/s41467-021-24551-5

Ek, M. B., & Holtslag, A. A. M. (2004). Influence of soil moisture on boundary layer cloud development. *Journal of Hydrometeorology*, *5*(1), 86–99. https://doi.org/10.1175/1525-7541(2004)005<0086:iosmob>2.0.co;2

Findell, K. L., & Eltahir, E. A. B. (2003). Atmospheric controls on soil moisture-boundary layer interactions. Part I: Framework development. *Journal of Hydrometeorology*, *4*(3), 552–569. https://doi.org/10.1175/1525-7541(2003)004<0552:acosml>2.0.co;2

Fisch, G., Tota, J., Machado, L. A. T., Silva Dias, M. A. F., da, R. F., Nobre, C. A., et al. (2004). The convective boundary layer over pasture and forest in Amazonia. *Theoretical and Applied Climatology*, *78*(1–3), 47–59. https://doi.org/10.1007/s00704-004-0043-x

Fulton, R. A., Breidenbach, J. P., Seo, D. J., Miller, D. A., & O'Bannon, T. (1998). The WSR-88D rainfall algorithm. *Weather and Forecasting*, *13*(2), 377–395. https://doi.org/10.1175/1520-0434(1998)013<0377:twra>2.0.co;2

Gambill, L. D., & Mecikalski, J. R. (2011). A Satellite-based summer convective cloud frequency analysis over the southeastern United States. *Journal of Applied Meteorology and Climatology*, *50*(8), 1756–1769. https://doi.org/10.1175/2010JAMC2559.1

Garcia-Carreras, L., Marsham, J. H., & Spracklen, D. V. (2017). Observations of increased cloud cover over irrigated agriculture in an arid environment. *Journal of Hydrometeorology*, *18*(8), 2161–2172. https://doi.org/10.1175/JHM-D-16-0208.1

Garcia-Carreras, L., Parker, D. J., & Marsham, J. H. (2011). What is the mechanism for the modification of convective cloud distributions by land surface-induced flows? *Journal of the Atmospheric Sciences*, *68*(3), 619–634. https://doi.org/10.1175/2010JAS3604.1

Garcia-Carreras, L., Parker, D. J., Taylor, C. M., Reeves, C. E., & Murphy, J. G. (2010). Impact of mesoscale vegetation heterogeneities on the dynamical and thermodynamic properties of the planetary boundary layer. *Journal of Geophysical Research*, *115*(3), D03102. https://doi.org/10.1029/2009JD012811

Gentine, P., Holtslag, A. A. M., D'Andrea, F., & Ek, M. (2013). Surface and atmospheric controls on the onset of moist convection over land. *Journal of Hydrometeorology*, *14*(5), 1443–1462. https://doi.org/10.1175/JHM-D-12-0137.1

Heiblum, R. H., Koren, I., & Feingold, G. (2014). On the link between Amazonian forest properties and shallow cumulus cloud fields. *Atmospheric Chemistry and Physics*, *14*(12), 6063–6074. https://doi.org/10.5194/acp-14-6063-2014

Heinze, R., Moseley, C., Böske, L. N., Muppa, S. K., Maurer, V., Raasch, S., & Stevens, B. (2017). Evaluation of large-eddy simulations forced with mesoscale model output for a multi-week period during a measurement campaign. *Atmospheric Chemistry and Physics*, *17*(11), 7083–7109. https://doi.org/10.5194/ACP-17-7083-2017

Kang, S. L., Davis, K. J., & LeMone, M. (2007). Observations of the ABL structures over a heterogeneous land surface during IHOP_2002. *Journal of Hydrometeorology*, *8*(2), 221–244. https://doi.org/10.1175/JHM567.1

Kassianov, E. I., Riley, E. A., Kleiss, J. M., Riihimaki, L. D., & Berg, L. K. (2019). Macrophysical properties of continental shallow cumuli: Diurnal evolution. In A. Comerón, E. I. Kassianov, K. Schäfer, R. H. Picard, K. Weber, & U. N. Singh (Eds.), *Remote Sensing of Clouds and the Atmosphere XXIV*, 11152, 9. SPIE-Intl Soc Optical Eng. https://doi.org/10.1117/12.2534359

Kulmala, M., Suni, T., Lehtinen, K. E. J., Dal Maso, M., Boy, M., Reissell, A., et al. (2004). A new feedback mechanism linking forests, aerosols, and climate. *Atmospheric Chemistry and Physics*, *4*(2), 557–562. https://doi.org/10.5194/acp-4-557-2004

Lamer, K., & Kollias, P. (2015). Observations of fair-weather cumuli over land: Dynamical factors controlling cloud size and cover. *Geophysical Research Letters*, *42*(20), 8693–8701. https://doi.org/10.1002/2015GL064534

Lareau, N. P., Zhang, Y., & Klein, S. A. (2018). Observed boundary layer controls on shallow cumulus at the ARM Southern Great Plains site. *Journal of the Atmospheric Sciences*, *75*(7), 2235–2255. https://doi.org/10.1175/JAS-D-17-0244.1

Lee, J. M., Zhang, Y., & Klein, S. A. (2019). The effect of land surface heterogeneity and background wind on shallow cumulus clouds and the transition to deeper convection. *Journal of the Atmospheric Sciences*, *76*(2), 401–419. https://doi.org/10.1175/JAS-D-18-0196.1

Lee, T. R., Buban, M., Turner, D. D., Meyers, T. P., & Baker, C. B. (2019). *Evaluation of the High-Resolution Rapid Refresh (HRRR) model using near-surface meteorological and flux observations from northern Alabama*. Weather and Forecasting. https://doi.org/10.1175/WAF-D-18-0184.1

Liu, G., Liu, Y., & Endo, S. (2013). Evaluation of surface flux parameterizations with long-term ARM observations. *Monthly Weather Review*, *141*(2), 773–797. https://doi.org/10.1175/MWR-D-12-00095.1

Lothon, M., Campistron, B., Chong, M., Couvreux, F., Guichard, F., Rio, C., & Williams, E. (2011). Life cycle of a mesoscale circular gust front observed by a C-band Doppler radar in West Africa. *Monthly Weather Review*, *139*(5), 1370–1388. https://doi.org/10.1175/2010MWR3480.1

Lyons, T. J., Schwerdtfeger, P., Hacker, J. M., Foster, I. J., Smith, R. C. G., & Huang, X. (1993). Land-atmosphere interaction in a semiarid region: The bunny fence experiment. *Bulletin of the American Meteorological Society*, *74*(7), 1327–1334. https://doi.org/10.1175/1520-0477(1993)074<1327:liiasr>2.0.co;2

Mahrt, L., & Ek, M. (1993). Spatial variability of turbulent fluxes and roughness lengths in HAPEX-MOBILHY. *Boundary-Layer Meteorology*, *65*(4), 381–400. https://doi.org/10.1007/BF00707034

Mahrt, L., Sun, J., Vickers, D., Macpherson, J. I., Pederson, J. R., & Desjardins, R. L. (1994). Observations of fluxes and inland breezes over a heterogeneous surface. *Journal of the Atmospheric Sciences*, *51*(17), 2484–2499. https://doi.org/10.1175/1520-0469(1994)051<2484:oofaib>2.0.co;2

Nair, U. S., Lawton, R. O., Welch, R. M., & Pielke, R. A. (2003). Impact of land use on Costa Rican tropical montane cloud forests: Sensitivity of cumulus cloud field characteristics to lowland deforestation. *Journal of Geophysical Research*, *108*(7), 4206. https://doi.org/10.1029/2001jd001135

Patton, E. G., Sullivan, P. P., & Moeng, C. H. (2005). The influence of idealized heterogeneity on wet and dry planetary boundary layers coupled to the land surface. *Journal of the Atmospheric Sciences*, *62*(7), 2078–2097. https://doi.org/10.1175/JAS3465.1

Peñuelas, J., & Staudt, M. (2010). BVOCs and global change. *Trends in plant science. Elsevier Current Trends*, *15*(3), 133–144. https://doi.org/10.1016/j.tplants.2009.12.005

Pielke, S. (2001). Influence of the spatial distribution of vegetation and soils on the prediction of cumulus convective rainfall. *Reviews of Geophysics*, *39*(2), 151–177. https://doi.org/10.1029/1999RG000072

Qiu, S., & Williams, I. N. (2020). Observational evidence of state-dependent positive and negative land surface feedback on afternoon deep convection over the Southern Great Plains. *Geophysical Research Letters*, *47*(5), 1–9. https://doi.org/10.1029/2019GL086622

Rabin, R. M., & Martin, D. W. (1996). Satellite observations of shallow cumulus coverage over the central United States: An exploration of land use impact on cloud cover. *Journal of Geophysical Research*, *101*(D3), 7149–7155. https://doi.org/10.1029/95JD02891

Rabin, R. M., Steven, S., Peter, J. W., David, J. S., & Gregory, M. (1990). Observed effects of landscape variability on convective clouds. *Bulletin of the American Meteorological Society*, *71*(3), 272–280. https://doi.org/10.1175/1520-0477(1990)071<0272:oeolvo>2.0.co;2

Ray, D. K., Nair, U. S., Welch, R. M., Han, Q., Zeng, J., Su, W., et al. (2003). Effects of land use in southwest Australia: 1. Observations of cumulus cloudiness and energy fluxes. *Journal of Geophysical Research*, *108*(14), 1–20. https://doi.org/10.1029/2002jd002654

Rieck, M., Hohenegger, C., & van Heerwaarden, C. C. (2014). The influence of land surface heterogeneities on cloud size development. *Monthly Weather Review*, *142*(10), 3830–3846. https://doi.org/10.1175/MWR-D-13-00354.1

Romps, D. M. (2017). Exact expression for the lifting condensation level. *Journal of the Atmospheric Sciences*, *74*(12), 3891–3900. https://doi.org/10.1175/JAS-D-17-0102.1

Romps, D. M., & Öktem, R. (2018). Observing clouds in 4d with multiview stereophotogrammetry. *Bulletin of the American Meteorological Society*, *99*(12), 2575–2586. https://doi.org/10.1175/BAMS-D-18-0029.1

Romps, D. M., Öktem, R., Endo, S., & Vogelmann, A. M. (2021). On the lifecycle of a shallow cumulus cloud: Is it a bubble or plume, active or forced? *Journal of the Atmospheric Sciences*, 1–20. https://doi.org/10.1175/jas-d-20-0361.1

Sakaguchi, K., Berg, L. K., Chen, J., Fast, J., Newsom, R., Tai, S.-L., et al. (2022). Determining spatial scales of soil moisture—Cloud coupling pathways using semi-idealized simulations. *Journal of Geophysical Research: Atmospheres*, *127*(2), e2021JD035282. https://doi.org/10.1029/2021JD035282

Schmit, T. J., Gunshor, M. M., Fu, G., Rink, T., Bah, K., & Wolf, W. (2010). *GOES-R advanced baseline imager (ABI) algorithm theoretical basis document for cloud and moisture imagery product*. Version 2.3, 62, Noaa Nesdis Star. Retrieved from https://www.star.nesdis.noaa.gov/goesr/documents/ATBDs/Baseline/ATBD_GOES-R_ABI_CMI_KPP_v3.0_July2012.pdf

Segal, M., Avissar, R., McCumber, M. C., & Pielke, R. A. (1988). Evaluation of vegetation effects on the generation and modification of mesoscale circulations. *Journal of the Atmospheric Sciences*, *45*(16), 2268–2292. https://doi.org/10.1175/1520-0469(1988)045<2268:eoveot>2.0.co;2

Simon, J. S., Bragg, A. D., Dirmeyer, P. A., & Chaney, N. W. (2021). Semi-coupling of a field-scale resolving land-surface model and WRF-LES to investigate the influence of land-surface heterogeneity on cloud development. *Journal of Advances in Modeling Earth Systems*, *13*(10), e2021MS002602. https://doi.org/10.1029/2021MS002602

Smith, T. L., Benjamin, S. G., Brown, J. M., Weygandt, S., Smirnova, T., & Schwartz, B. (2008). Convection forecasts from the hourly updated, 3-km high resolution rapid refresh (HRRR) model. *24th Conference on Severe Local Storms*.

Song, F., Feng, Z., Ruby Leung, L., Houze, R. A., Wang, J., Hardin, J., & Homeyer, C. R. (2019). Contrasting spring and summer large-scale environments associated with mesoscale convective systems over the U.S. Great Plains. *Journal of Climate*, *32*(20), 6749–6767. https://doi.org/10.1175/JCLI-D-18-0839.1

Tang, Q., Xie, S., Zhang, Y., Phillips, T. J., Santanello, J. A., Cook, D. R., et al. (2018). Heterogeneity in warm-season land-atmosphere coupling over the U.S. Southern Great Plains. *Journal of Geophysical Research: Atmospheres*, *123*(15), 7867–7882. https://doi.org/10.1029/2018JD028463

Tang, S., Xie, S., Zhang, M., Tang, Q., Zhang, Y., Klein, S. A., et al. (2019). Differences in eddy-correlation and energy-balance surface turbulent heat flux measurements and their impacts on the large-scale forcing fields at the ARM SGP site. *Journal of Geophysical Research: Atmospheres*, *124*(6), 3301–3318. https://doi.org/10.1029/2018JD029689

Tao, C., Zhang, Y., Tang, Q., Ma, H.-Y., Ghate, V. P., Tang, S., et al. (2021). Land–Atmosphere coupling at the U.S. Southern Great Plains: A comparison on local convective regimes between ARM observations, reanalysis, and climate model simulations. *Journal of Hydrometeorology*, *22*(2), 463–481. https://doi.org/10.1175/jhm-d-20-0078.1

Tao, C., Zhang, Y., Tang, S., Tang, Q., Ma, H. Y., Xie, S., & Zhang, M. (2019). Regional moisture budget and land-atmosphere coupling over the U.S. Southern Great Plains inferred from the ARM long-term observations. *Journal of Geophysical Research: Atmospheres*, *124*(17–18), 10091–10108. https://doi.org/10.1029/2019JD030585

Taylor, C. M., De Jeu, R. A. M., Guichard, F., Harris, P. P., & Dorigo, W. A. (2012). Afternoon rain more likely over drier soils. *Nature*, *489*(7416), 423–426. https://doi.org/10.1038/nature11377

Taylor, C. M., Gounou, A., Guichard, F., Harris, P. P., Ellis, R. J., Couvreux, F., & De Kauwe, M. (2011). Frequency of sahelian storm initiation enhanced over mesoscale soil-moisture patterns. *Nature Geoscience*, *4*(7), 430–433. https://doi.org/10.1038/ngeo1173

Taylor, C. M., Parker, D. J., & Harris, P. P. (2007). An observational case study of mesoscale atmospheric circulations induced by soil moisture. *Geophysical Research Letters*, *34*(15), 2–7. https://doi.org/10.1029/2007GL030572

Teuling, A. J., Seneviratne, S. I., Stöckli, R., Reichstein, M., Moors, E., Ciais, P., et al. (2010). Contrasting response of European forest and grassland energy exchange to heatwaves. *Nature Geoscience*, *3*(10), 722–727. https://doi.org/10.1038/ngeo950

Teuling, A. J., Taylor, C. M., Meirink, J. F., Melsen, L. A., Miralles, D. G., Van Heerwaarden, C. C., et al. (2017). Observational evidence for cloud cover enhancement over Western European forests. *Nature Communications*, *8*, 1–7. https://doi.org/10.1038/ncomms14065

Theeuwes, N. E., Barlow, J. F., Teuling, A. J., Grimmond, C. S. B., & Kotthaus, S. (2019). Persistent cloud cover over mega-cities linked to surface heat release. *Npj Climate and Atmospheric Science*, *2*(1). https://doi.org/10.1038/s41612-019-0072-x

Tian, J., Zhang, Y., Klein, S. A., Wang, L., & Öktem, R. (2021). *Summertime continental shallow cumulus cloud detection using GOES-16 satellite and ground-based stereo cameras at the DOE ARM Southern Great Plains site*.

Van Heerwaarden, C. C., & Teuling, A. J. (2014). Disentangling the response of forest and grassland energy exchange to heatwaves under idealized land-atmosphere coupling. *Biogeosciences*, *11*(21), 6159–6171. https://doi.org/10.5194/bg-11-6159-2014

Walker, J. R., Mecikalski, J. R., Knupp, K. R., & MacKenzie, W. M. (2009). Development of a land surface heating index-based method to locate regions of potential mesoscale circulation formation. *Journal of Geophysical Research*, *114*(16), 1–11. https://doi.org/10.1029/2009JD011853

Wang, J., Chagnon, F. J. F., Williams, E. R., Betts, A. K., Renno, N. O., Machado, L. A. T., et al. (2009). Impact of deforestation in the Amazon basin on cloud climatology. *Proceedings of the National Academy of Sciences of the United States of America*, *106*(10), 3670–3674. https://doi.org/10.1073/pnas.0810156106

Wang, Y., Zeng, X., Xu, X., Welty, J., Lenschow, D. H., Zhou, M., & Zhao, Y. (2020). Why are there more summer afternoon low clouds over the Tibetan Plateau compared to eastern China? *Geophysical Research Letters*, *47*(23), e2020GL089665. https://doi.org/10.1029/2020GL089665

Weaver, C. P., & Avissar, R. (2001). Atmospheric disturbances caused by human modification of the landscape. *Bulletin of the American Meteorological Society*, *82*(2), 269–281. https://doi.org/10.1175/1520-0477(2001)082<0269:adcbhm>2.3.co;2

Wilde, N. P., Stull, R. B., & Eloranta, E. W. (1985). The LCL zone and cumulus onset. *Journal of Applied Meteorology and Climatology*, *24*(7), 640–657. https://doi.org/10.1175/1520-0450(1985)024<0640:tlzaco>2.0.co;2

Wu, X., & Schmit, T. (2019). *GOES-16 ABI level 1b and cloud and moisture imagery (CMI) release full validation data quality product performance guide for data users*. (Cmi).

Xiao, H., Berg, L. K., & Huang, M. (2018). The impact of surface heterogeneities and land-atmosphere interactions on shallow clouds over ARM SGP site. *Journal of Advances in Modeling Earth Systems*, *10*(6), 1220–1244. https://doi.org/10.1029/2018MS001286

Xu, R., Li, Y., Teuling, A. J., Zhao, L., Garcia-carreras, L., Meier, R., et al. (2022). Contrasting impacts of forests on cloud cover based on satellite observations. *Nature Communications*, *13*, 670. https://doi.org/10.1038/s41467-022-28161-7

Zhang, Y., & Klein, S. A. (2010). Mechanisms affecting the transition from shallow to deep convection over land: Inferences from observations of the diurnal cycle collected at the ARM Southern Great Plains site. *Journal of the Atmospheric Sciences*, *67*(9), 2943–2959. https://doi.org/10.1175/2010JAS3366.1

Zhang, Y., & Klein, S. A. (2013). Factors controlling the vertical extent of fair-weather shallow cumulus clouds over land: Investigation of diurnal-cycle observations collected at the ARM Southern Great Plains site. *Journal of the Atmospheric Sciences*, *70*(4), 1297–1315. https://doi.org/10.1175/JAS-D-12-0131.1

Zhang, Y., Klein, S. A., Fan, J., Chandra, A. S., Kollias, P., Xie, S., & Tang, S. (2017). Large-eddy simulation of shallow cumulus over land: A composite case based on ARM long-term observations at its Southern Great Plains site. *Journal of the Atmospheric Sciences*, *74*(10), 3229–3251. https://doi.org/10.1175/JAS-D-16-0317.1

Zhong, S., & Doran, J. C. (1997). A study of the effects of spatially varying fluxes on cloud formation and boundary layer properties using data from the Southern Great Plains Cloud and Radiation Testbed. *Journal of Climate*, *10*(2), 327–341. https://doi.org/10.1175/1520-0442(1997)010<0327:asoteo>2.0.co;2